Vacuum 175 (2020) 109255

Contents lists available at ScienceDirect

Vacuum

journal homepage: http://www.elsevier.com/locate/vacuum

Synthesis of Gd_2O_3/CdO composite by sol-gel method: Structural, morphological, optical, electrochemical and magnetic studies

Ramesh Sivasamy [a,c,*], Potu Venugopal [b], Edgar Mosquera [d,e]

[a] Department of Chemical Engineering, Biotechnology and Materials, University of Chile, Beauchef 851, Santiago, Chile
[b] Department of Chemistry, Pondicherry University, Pondicherry, 605014, India
[c] Saveetha School of Engineering, Saveetha University, Chennai, Tamilnadu, 602105, India
[d] Departamento de Física, Universidad Del Valle, A.A, 25360, Cali, Colombia
[e] Centro de Excelencia en Nuevos Materiales, Universidad Del Valle, A.A, 25360, Cali, Colombia

ARTICLE INFO

Keywords:
Composite
Sol-gel synthesis
Rietveld refinement
Optical energy band gap
Cyclic voltammetry
Paramagnetic behavior

ABSTRACT

Metal-oxide based hybrid composite materials have broad applications in optical and electrochemical applications. Hence, in this present work fabrication of multifunctional Gd_2O_3/CdO composite using the facile sol-gel method. The crystalline structure, surface morphology, optical, electrochemical and magnetic behavior were studied. The composite formation, phase identification and crystalline structures of the cubic crystalline Gd_2O_3 and CdO particles of the composite were confirmed by the X-ray diffraction. Surface morphology and chemical composition analysis were examined using scanning electron microscopy with energy dispersive X-ray analysis. The optical energy band-gap of the composite from the diffuse reflectance spectra is found to be 1.27 eV and 2.76 eV. The electrochemical performance was estimated from the cyclic voltammetry analysis. The symmetric nature of the voltammetry curve shows that this composite is a promising entrant for fast redox reactions with enhanced specific capacitance. The magnetization curve explores the sample behaves as paramagnetic at room temperature.

1. Introduction

Transition metal oxide multifunctional hybrid composite materials have attracted much attention due to their interesting properties such as electrical, catalytic, magnetic, optical, and structural stability [1–3]. The multifunctional composites were desired because of their integrated properties in a single material which often suitable for the futuristic development in device miniaturization in several industrial applications [4,5]. At present, energy storage and conversion are the great challenges to advanced technology due to their high energy-consuming ability [6]. Henceforth, the researchers have concentrated on a wide range of multifunctional high-efficiency, environment-friendly and cost-effective composite materials for the photocatalytic and electrochemical applications [7,8].

Rare earth compounds with elements such as Nd, Gd, Eu, and Er are characterized by multiple absorption energy levels in the ultraviolet (UV) and visible range. The gadolinium oxide (Gd_2O_3) shows an interesting optical and magnetic property that is used in several industrial applications such as magnetic resonance imaging, catalytic, luminescent devices and magnetocaloric materials [9,10]. Besides, the gadolinium element with a half-filled 4f-shell and 5d orbitals which offers to inter (4f-5d), intra (5d-5d) interaction through charge carriers and the empty 5d shell behave as a trapping center to prevent the recombination of carriers for the visible light photocatalytic activities [11,12].

However, using a single metal oxide may not be more effective because of their poor visual light absorption and the rapid recombination process affects their properties. The low light harvesting, and charge recombination process are the main issues to affect the photoelectrode, photovoltaic and catalytic applications of the nanoparticles.

To overcome these issues, two or more materials combined to produce a composite material with new properties for multifunctional applications [13,14]. The hybrid metal oxide composite materials can alter the band-gap and enhancing the visible light absorption. There are several reports are presented to enhance the properties of the material by making composites with different materials [15–19].

Among the several transition metal oxide semiconductors, cadmium

* Corresponding author. Nanoscale Functional Materials Laboratory, Department of Chemical Engineering, Biotechnology and Materials, University of Chile, Floor 5, Office 533, Beauchef 851, Santiago, Chile.
E-mail addresses: rsivasamy@ing.uchile.cl, rameshsiva_chem@yahoo.com (R. Sivasamy).

https://doi.org/10.1016/j.vacuum.2020.109255
Received 28 November 2019; Received in revised form 5 February 2020; Accepted 10 February 2020
Available online 12 February 2020

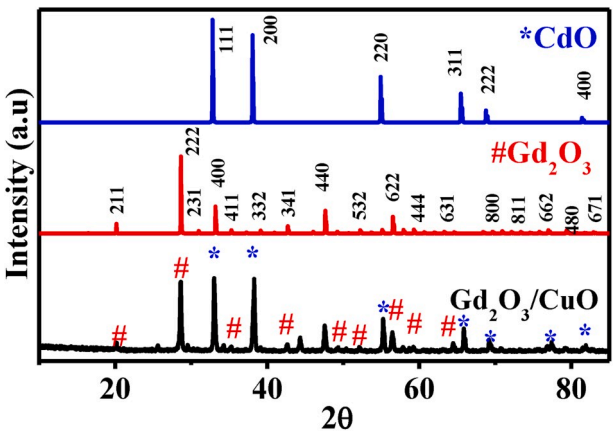

Fig. 1. Powder X-ray diffraction patterns of Gd_2O_3/CdO composite.

oxide (CdO) is a n-type (II-VI) semiconductor with the band-gap value of 2.5 eV have been used for photovoltaic cells, transparent electrodes, photodiodes, phototransistors, IR detectors, liquid crystal displays, and sensors because of their properties such as low resistivity, optimum refractive index, suitable band-gap, high carrier mobility, optical transparency, chemical stability, and low-cost material [20,21].

Thus, in this work, we synthesize a Gd_2O_3/CdO hybrid composite by a facile sol-gel method and studied their structure, morphology, optical, electrochemical, and magnetic properties.

2. Experimental

2.1. Synthesis of Gd_2O_3/CdO composite

The Gd_2O_3/CdO composite was synthesized using a simple sol-gel method via the nitrate-citrate route. Calculated amounts of reagent grade solutions of cadmium nitrate tetrahydrate ($CdN_2O_6.4H_2O$; 99.9%; Himedia) and gadolinium nitrate ($Gd(NO_3)_3$) were kept stirring separately. The $Gd(NO_3)_3$ was prepared using the gadolinium oxide (Gd_2O_3; 99.90%; Himedia) mixed with nitric acid (2 M) and stirred well for 15 min followed by 50 ml of 2 M citric acid solution ($C_6H_8O_7$; 99.7% Himedia) was added. Then the pH of the solution was adjusted to ~7 using the liquid ammonia. The resultant solution was kept stirring for 160 h, at ~45 °C to form a gel, then the gel was decomposed at ~100 °C to get the powder and finally, it was sintered at 600 °C for 6 h to achieve polycrystalline Gd_2O_3/CdO composite. The systematic preparation is presented with supporting information (Fig. S1).

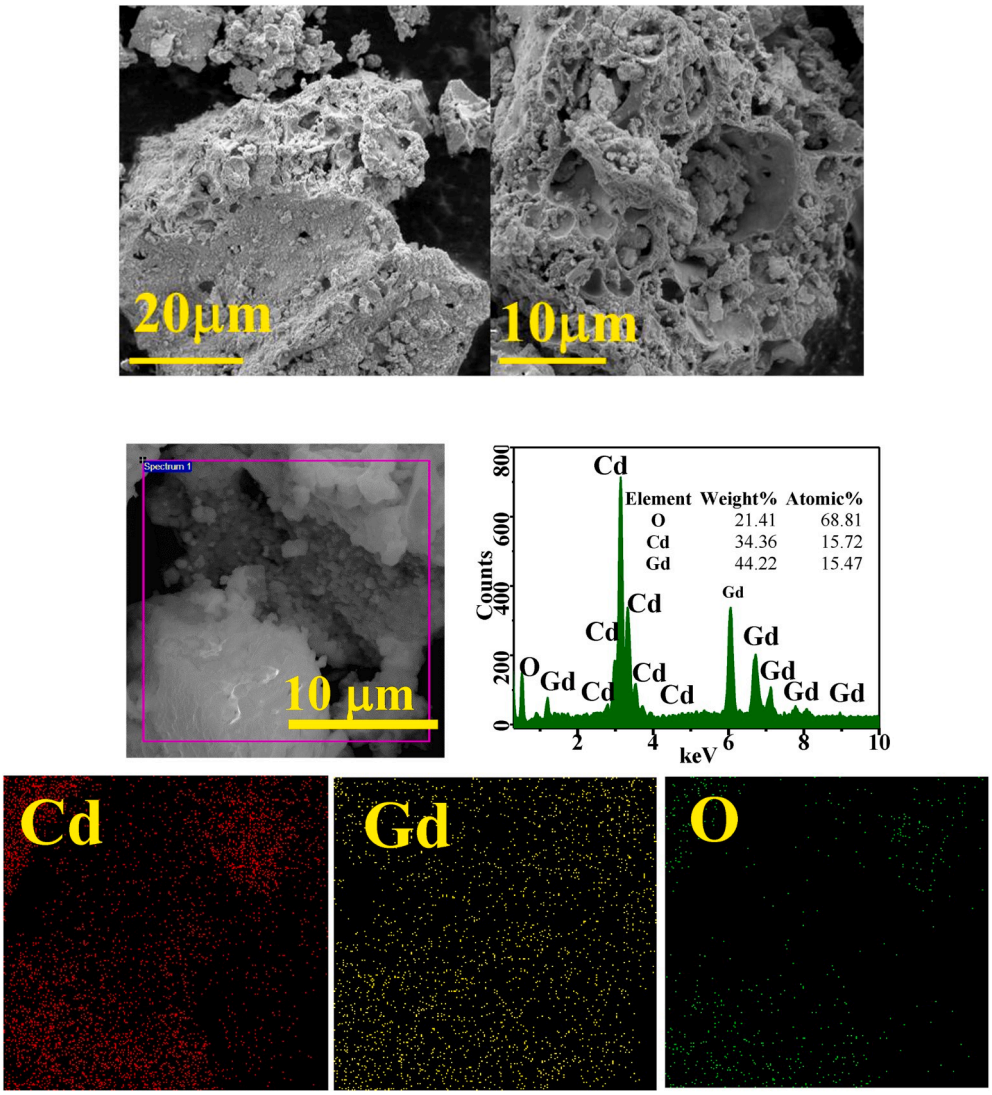

Fig. 2. SEM images (up), EDX profile (middle) and X-ray mapping (down) of Gd_2O_3/CdO composite.

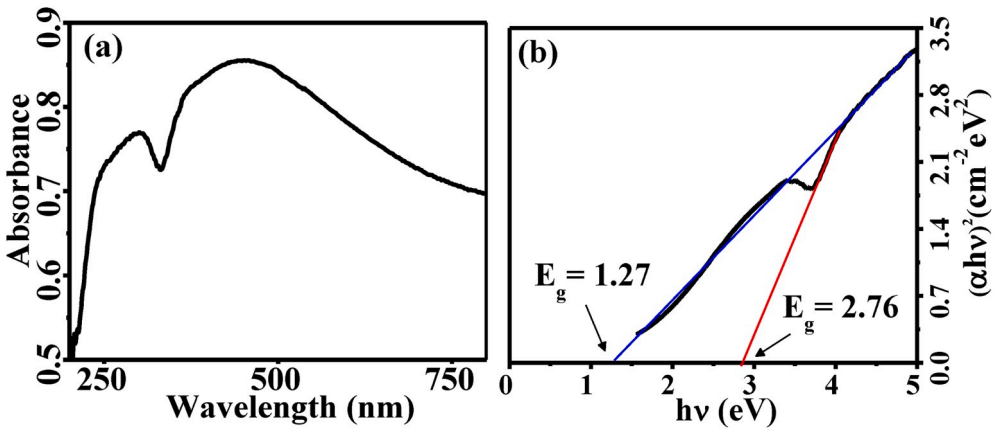

Fig. 3. (a) UV–Vis DRS spectra, and (b) Tauc plot of Gd_2O_3/CdO composite.

2.2. Characterizations

Phase identification and the structural information of the composite were revealed using room temperature powder X'Pert PRO PANalytical diffractometer with $Cu_{K\alpha}$ as a source which was operated at 40 kV/30 mA power. The surface morphology and the chemical composition was examined using the Hitachi-S3000H scanning electron microscopy with energy-dispersive X-ray spectroscopy (SEM-EDX). Electrochemical behavior was observed from the cyclic voltammetry (CV) curve using a three-electrode system. In the three-electrode system, the Pt wire and KCl-saturated Ag/AgCl are used as a counter and reference electrodes. The working electrode was prepared using a mixture of the Gd_2O_3/CdO composite, carbon powders and polyvinylidene fluoride (PVDF) with the ratio of 85:5:5 to confirm the conductivity. The 1 M aq. KOH was used as an electrolyte in the measurements. Magnetic behavior was identified using a LAKESHORE VSM 7404 vibrating sample magnetometer (VSM).

3. Results and discussions

3.1. X-ray diffraction studies

The phase identity, crystallite structure, and sizes of the synthesized Gd_2O_3/CdO composite were investigated by XRD. Fig. 1 shows the XRD pattern of Gd_2O_3/CdO composite compared with the simulated XRD patterns of CdO and Gd_2O_3 structures. The predominant peaks in the experimental pattern are in good agreement with the simulated CdO and Gd_2O_3 patterns. The diffraction peaks at 32.81, 38.13, 54.87, 65.51, 68.86, and 81.46 correspond to 111, 200, 220, 311, 222, and 400 planes which belong to a cubic lattice with *Fm*-3*m* (225) space group of CdO (Phase-1). The rest of the diffraction peaks at 20.21, 28.48, 33.21, 42.66 47.59, 56.65, 69.65 and 82.65 corresponds to the lattice planes of 211, 222, 400, 341, 440, 622, 800, 662, and 671 which corresponds to a cubic lattice type with $I2_13$ (199) space group of Gd_2O_3 (Phase-2). The XRD pattern of the as-synthesized sample reveals the existence of both phases and the peaks do not affect each other which confirms the formation of Gd_2O_3/CdO composite. The phase-1 and phase-2 are present in the composite of 45.81% and 54.19% respectively.

The average crystallite size of the composite from XRD peaks was obtained using the Debye-Scherrer formula (Eq. (1)) [17,22].

$$D = K\lambda/\beta\cos\theta \quad (1)$$

where D stands for crystallite size, K denotes Scherrer constant, λ meant for $Cu_{K\alpha}$ radiation, β is full width half maximum of the peak, and θ represents Bragg angle. The calculated average crystallite sizes of the phase-1 are found to be 386 nm and the phase-2 is 257 nm.

Rietveld analysis for structural refinement was carried out using the FullProf package [23]. The pseudo-Voigt function was used for profile fitting. The structural refinement converged for two-phase system of CdO and Gd_2O_3 cubic lattice type. The crystal structures of the two phases are shown in Supplementary Information Fig. S3. In CdO crystal structure (phase-1), the Cd atoms are placed in the Wyckoff positions of 4*b*, and the O atoms at the 4*a* position. In Gd_2O_3 structure (phase-2), Gd atoms are occupied in 12*b* and 8*a* positions and the O atoms at the 24*c* position. Rietveld refinement, XRD profile fit, and crystal information were listed in supporting information (Fig. S3, Tables T1, T2 and T3).

3.2. Electron microscopy

The SEM-EDX was used to get the surface morphology and composition of the Gd_2O_3/CdO composite. Fig. 2 shows the SEM micrographs and EDX-profile of the sample. The composite shows agglomeration and the morphology was found to be irregular with rough surface. The EDX-profile and X-Ray mapping of the composite show that the constituent elements are present without impurities and distributed throughout the surfaces.

3.3. Optical absorbance studies

The optical absorbance spectrum of the Gd_2O_3/CdO composite is shown in Fig. 3 (a). Here, we considered all transitions of the Gd_2O_3/CdO sample. Therefore, in the nanocomposite, the Gd_2O_3 nanoparticles show an indirect transition while CdO nanoparticles exhibit both, an indirect transition and direct transition. Thus, Fig. 3(a) shows a strong photon absorption around 300 nm (4.13 eV) and 453 nm (2.74 eV), respectively. The absorbance band at 300 nm (4.13 eV) is attributed to $^8S_{7/2} \rightarrow {}^6I_J$ (f-f) transitions of Gd^{3+} ions in Gd_2O_3 (Gd^{3+}; $4f^7$ electrons). This transition shows redshift (Δ = 0.97 eV) with respect to reported Gd_2O_3 (5.1 eV) [19]. Instead, the absorbance band at 453 nm (2.74 eV) corresponds to the direct transition of CdO crystallites present in the nanocomposite and which is slightly show a blueshift (Δ = 0.23 eV).

On the other hand, the Tauc's plot [6] have been used to verify the nature of the optical transition of the sample. The relation is written as Eq. (2):

$$\alpha h\upsilon = A(h\upsilon - E_g)^n \quad (2)$$

where E_g-energy band gap, α-absorption coefficient, hυ-photon energy, A-constant, and n is the transition types. Here, the direct transition (n = 1/2) has been considered and two energy band gaps at 1.27 eV and 2.76 eV are observed in the composite, Fig. 3 (b). The calculated energy band gap of the composite is found to be 1.27 eV which is narrower than the constituent oxides such as Gd_2O_3 (5.1 eV) [24] and CdO (1.98 eV, 2.51 eV) [20]. Therefore, the energy band gap of 1.27 eV (Δ = 0.71 eV) and 2.76 eV (Δ = 0.25 eV) could be related to the indirect and direct transition of CdO nanocrystals in the composite. Additionally, it was

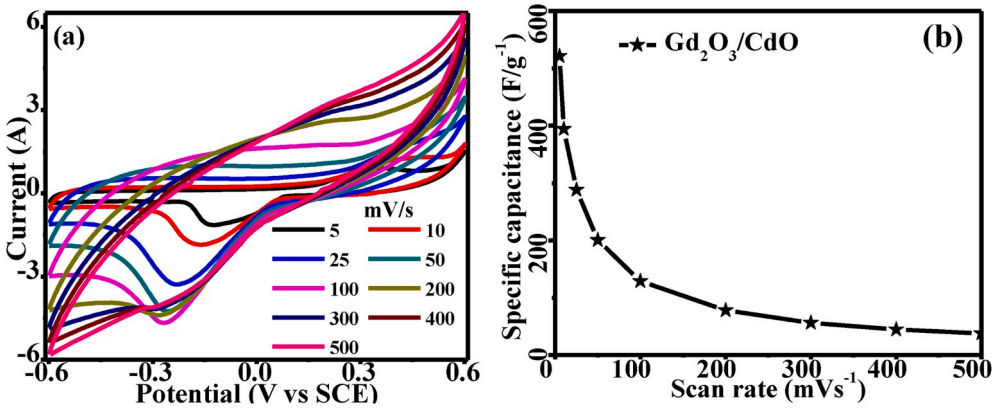

Fig. 4. (a) Cyclic voltammetry at different scanning rates, and (b) specific capacitance plot of Gd_2O_3/CdO composite.

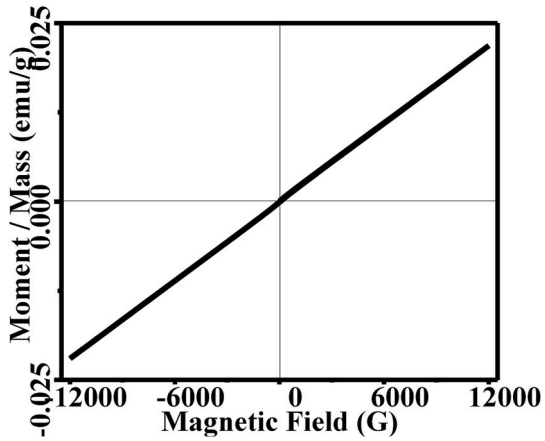

Fig. 5. Magnetization (M − H) plots of Gd_2O_3/CdO composite.

observed that the composite presents an indirect transition with redshift compared to that of CdO and Gd_2O_3 reported. In a previous report, Mosquera et al. studied the energy band gap in CdO/ZnO composites and found a slight redshift with the CdO content [20]. These results confirm that CdO may have an indirect optical transition at lower the direct absorption edge of 2.20 eV, thus the redshift can be attributed to the indirect optical transition. Concerning the above, the variation in the energy band gap suggests that this like composite-type can be used as catalysts in oxygen and hydrogen evolution electrochemical reactions.

3.4. Electrochemical studies

Electrochemical properties were examined using cyclic voltammetry (CV) experiments. The CV curves of Gd_2O_3/CdO composite was observed in the potential range from −0.61 V to 0.61 V at various scanning rate. The CV curves of the sample are shown in Fig. 4 (a). The separate anodic and cathodic peaks about 0.342 V and −0.124 V are due to the Cd^{2+}/Gd^{3+} to Cd/Gd^0 reversible conversion. Throughout the scan rate increases, it also increases the current density. The current density increases and the quasi-rectangular shape CV curves indicate that the composite has the pseudocapacitive behavior with the high surface area. The composite favorable for the fast-redox reactions [25–27].

The specific capacitance (Cs, F g^{-1}) of the composite was estimated from the CV curves using the following relation given below in Eq. (3) [28].

$$Cs = 1 \Big/ (\nu\omega(\Delta V)) \int_{V_a}^{V_c} iVdV \quad (3)$$

where Cs denotes specific capacitance (Cs, Fg^{-1}), v signifies scan rate (mVs^{-1}), ω indicates sample weight (g), and ΔV represents applied potential range (Va to Vc). The specific capacitance of as-synthesized of Gd_2O_3/CdO composite is 521 Fg^{-1} at a scan rate of 5 mVs^{-1} is shown in Fig. 4 (b). The reported specific capacitance of the CdO and Gd_2O_3 nanoparticles are 380 Fg^{-1} and 580 Fg^{-1} respectively [29,30]. Hence the synthesized Gd_2O_3/CdO composite is higher than recently reported constituent nanoparticles. The synergetic effects of the composite formation enable the enhanced specific capacity of the sample.

3.5. Magnetic studies

Fig. 5 illustrates the magnetization curve of Gd_2O_3/CdO composite was recorded in the range of ±12000 G at 300 K. The magnetization versus magnetic field curve indicates that the composite is paramagnetic. Magnetic susceptibility, (χ) of the sample was calculated according to the relation below (Eq. (4)) [4].

$$M = \chi H \quad (4)$$

where M denotes magnetization (emu g^{-1}) and H is applied magnetic field. The calculated magnetic susceptibility of the composite is 1.857 $x10^{-6}$ emu/g which further confirms the paramagnetic behavior at 300 K.

4. Conclusion

In summary, the multifunctional cubic lattice Gd_2O_3/CdO composite was successfully synthesized by the sol-gel method. The calculated optical energy band-gap energy is 1.27 eV which shows a strong redshift in the energy band-gap with respect to the CdO and Gd_2O_3 reported. The CV curves indicate that the reversible redox process implicate in the system. The specific capacitance of the composite is found to be 521 Fg−1 at a scan rate of 5 mVs^{-1} which is higher than the reported CdO and Gd_2O_3 oxides. The shape of the magnetization curve reveals that the composite is paramagnetic at 300 K. The estimated narrow optical energy band-gap, specific capacitance and the magnetic properties of the composite can offer this material as a magnetically mediated electrophoto catalyst under visible light region which can be explored in future.

Declaration of competing interest

The authors declare that they have no known competing financial interests or personal relationships that could have appeared to influence the work reported in this paper.

Acknowledgment

The author Ramesh Sivasamy is thankful to the National Fund for

Scientific and Technological Development (FONDECYT) for the Grant number 3170052.

Appendix A. Supplementary data

Supplementary data to this article can be found online at https://doi.org/10.1016/j.vacuum.2020.109255.

References

[1] Y. Li, Z.G. Yu, L. Wang, Y. Weng, C.S. Tang, X. Yin, K. Han, H. Wu, X. Yu, L. M. Wong, D. Wan, X.R. Wang, J. Chai, Y.-W. Zhang, S. Wang, J. Wang, A.T.S. Wee, M.B.H. Breese, S.J. Pennycook, T. Venkatesan, S. Dong, J.M. Xue, J. Chen, Electronic-reconstruction-enhanced hydrogen evolution catalysis in oxide polymorphs, Nat. Commun. 10 (1) (2019) 3149.

[2] S. Sikarwar, B.C. Yadav, R.K. Sonker, G.I. Dzhardimalieva, J.K. Rajput, Synthesis and characterization of highly porous hexagonal shaped CeO_2-Gd_2O_3-CoO nanocomposite and its opto-electronic humidity sensing, Appl. Surf. Sci. 479 (2019) 326–333.

[3] Y. Zhu, H.A. Tahini, Z. Hu, J. Dai, Y. Chen, H. Sun, W. Zhou, M. Liu, S.C. Smith, H. Wang, Z. Shao, Unusual synergistic effect in layered Ruddlesden−Popper oxide enables ultrafast hydrogen evolution, Nat. Commun. 10 (1) (2019) 149.

[4] S. Ramesh, J.V. Ramaclus, E. Mosquera, B.B. Das, Sol–gel synthesis, structural, optical and magnetic characterization of $Ag_{3(2+x)}Pr_xNb_{4-x}O_{11+\delta}$ ($0.0 \leq x \leq 1.0$) nanoparticles, RSC Adv. 6 (8) (2016) 6336–6341.

[5] S. Ramesh, J.V. Ramaclus, B.B. Das, E. Mosquera, Structural, morphological, optical and magnetic properties of $Ag_{3(2+x)}In_xNb_{4-x}O_{11+\delta}$ ($0.25 \leq x \leq 1.0$) nanoparticles synthesized by sol–gel method, Mater. Res. Bull. 105 (2018) 121–125.

[6] B.J. Rani, G. Ravi, R. Yuvakkumar, S.I. Hong, Novel $SmMn_2O_5$ hollow long nanocuboids for electrochemical supercapacitor and water splitting applications, Vacuum 166 (2019) 279–285.

[7] Z. Shi, L. Lan, Y. Li, Y. Yang, Q. Zhang, J. Wu, G. Zhang, X. Zhao, Co_3O_4/TiO_2 nanocomposite formation leads to improvement in ultraviolet–visible-infrared-driven thermocatalytic activity due to photoactivation and photocatalysis–thermocatalysis synergetic effect, ACS Sustain. Chem. Eng. 6 (12) (2018) 16503–16514.

[8] S. Ramesh, P. Venugopal, E. Mosquera, Experimental and theoretical investigation of Bixbyite $(Mn_{0.8}Ni_{0.2})_2O_3$ nanoparticles for magnetic and electrochemical applications, J. Magn. Magn Mater. 443 (2017) 45–50.

[9] D.A. Zatsepin, D.W. Boukhvalov, A.F. Zatsepin, Y.A. Kuznetsova, M. A. Mashkovtsev, V.N. Rychkov, V.Y. Shur, A.A. Esin, E.Z. Kurmaev, Electronic structure, charge transfer, and intrinsic luminescence of gadolinium oxide nanoparticles: experiment and theory, Appl. Surf. Sci. 436 (2018) 697–707.

[10] R. Sivasamy, P. Venugopal, R. Espinoza-González, Crystal structure, optical and magnetic properties of perovskite $Gd(Mn_{0.7}Ni_{0.3})O_3$ ceramic nanoparticles: an experimental and first-principles studies, Ceram. Int. 45 (16) (2019) 20022–20027.

[11] H. Liu, G. Liu, G. Xie, M. Zhang, Z. Hou, Z. He, Gd^{3+}, N-codoped trititanate nanotubes: preparation, characterization and photocatalytic activity, Appl. Surf. Sci. 257 (8) (2011) 3728–3732.

[12] B. Frietsch, J. Bowlan, R. Carley, M. Teichmann, S. Wienholdt, D. Hinzke, U. Nowak, K. Carva, P.M. Oppeneer, M. Weinelt, Disparate ultrafast dynamics of itinerant and localized magnetic moments in gadolinium metal, Nat. Commun. 6 (2015) 8262.

[13] A. Ziarati Saravani, M. Nadimi, M.A. Aroon, A. Ebrahimian Pirbazari, Magnetic TiO_2/$NiFe_2O_4$/reduced graphene oxide nanocomposite as a recyclable photocatalyst for photocatalytic removal of methylene blue under visible light, J. Alloys Compd. 803 (2019) 291–306.

[14] P.M. Ajayan, J.M. Tour, Nanotube composites, Nature 447 (2007) 1066.

[15] Y. He, R. Wang, T. Jiao, X. Yan, M. Wang, L. Zhang, Z. Bai, Q. Zhang, Q. Peng, Facile preparation of self-assembled layered double hydroxide-based composite dye films as new chemical gas sensors, ACS Sustain. Chem. Eng. 7 (12) (2019) 10888–10899.

[16] J. Zhu, R. Wang, R. Geng, X. Zhang, F. Wang, T. Jiao, J. Yang, Z. Bai, Q. Peng, A facile preparation method for new two-component supramolecular hydrogels and their performances in adsorption, catalysis, and stimuli-response, RSC Adv. 9 (39) (2019) 22551–22558.

[17] S. Ramesh, Sol-Gel Synthesis and Characterization of $Ag_{3(2+x)}Al_xTi_{4-x}O_{11+\delta}$ ($0.0 \subseteq x \supseteq 1.0$) Nanoparticles, J. Nanosci. (2013) 1–9, https://doi.org/10.1155/2013/929321, 929321.

[18] J. Tian, Q. Shao, J. Zhao, D. Pan, M. Dong, C. Jia, T. Ding, T. Wu, Z. Guo, Microwave solvothermal carboxymethyl chitosan templated synthesis of TiO_2/ZrO_2 composites toward enhanced photocatalytic degradation of Rhodamine B, J. Colloid Interface Sci. 541 (2019) 18–29.

[19] J.Y. Chu, K.H. Lee, A.R. Kim, D.J. Yoo, Graphene-mediated organic-inorganic composites with improved hydroxide conductivity and outstanding alkaline stability for anion exchange membranes, Compos. B Eng. 164 (2019) 324–332.

[20] E. Mosquera, I. del Pozo, M. Morel, Structure and red shift of optical band gap in CdO–ZnO nanocomposite synthesized by the sol gel method, J. Solid State Chem. 206 (2013) 265–271.

[21] H. Güney, The structural, morphological, optical and electrical properties of Pb doped CdO thin films grown by spray method, Vacuum 159 (2019) 261–268.

[22] S. Ramesh, B.B. Das, Synthesis, structure and characterization of $Nd_{2X}Cd_{2-3X}SiO_4$ ($0.01 \leq X \leq 0.21$) solid-solutions, J. Kor. Chem. Soc. 55 (3) (2011) 7.

[23] J. Rodríguez-Carvajal, Recent advances in magnetic structure determination by neutron powder diffraction, Phys. B Condens. Matter 192 (1) (1993) 55–69.

[24] X. Jiang, L. Yu, C. Yao, F. Zhang, J. Zhang, C. Li, Synthesis and characterization of Gd_zO_3 hollow microspheres using a template-directed method, Materials 9 (5) (2016) 323.

[25] Y. Xu, J. Wei, L. Tan, J. Yu, Y. Chen, A Facile approach to $NiCoO_2$ intimately standing on nitrogen doped graphene sheets by one-step hydrothermal synthesis for supercapacitors, J. Mater. Chem. 3 (13) (2015) 7121–7131.

[26] L. Xuan, L. Chen, Q. Yang, W. Chen, X. Hou, Y. Jiang, Q. Zhang, Y. Yuan, Engineering 2D multi-layer graphene-like Co_3O_4 thin sheets with vertically aligned nanosheets as basic building units for advanced pseudocapacitor materials, J. Mater. Chem. 3 (34) (2015) 17525–17533.

[27] Y. Zhu, C. Cao, S. Tao, W. Chu, Z. Wu, Y. Li, Ultrathin nickel hydroxide and oxide nanosheets: synthesis, characterizations and excellent supercapacitor performances, Sci. Rep. 4 (2014) 5787.

[28] Z. Wu, X.-L. Huang, Z.-L. Wang, J.-J. Xu, H.-G. Wang, X.-B. Zhang, Electrostatic induced stretch growth of homogeneous β-$Ni(OH)_2$ on graphene with enhanced high-rate cycling for supercapacitors, Sci. Rep. 4 (2014) 3669.

[29] H.U. Shah, F. Wang, A.M. Toufiq, S. Ali, Z.U.H. Khan, Y. Li, J. Hu, K. He, Electrochemical properties of controlled size Mn_3O_4 nanoparticles for supercapacitor applications, J. Nanosci. Nanotechnol. 18 (1) (2018) 719–724.

[30] A.A. Yadav, S.N. Jadhav, D.M. Chougule, P.D. Patil, U.J. Chavan, Y.D. Kolekar, Spray deposited Hausmannite Mn_3O_4 thin films using aqueous/organic solvent mixture for supercapacitor applications, Electrochim. Acta 206 (2016) 134–142.